The Investigation of Surface Morphology Forming Mechanisms in Electropolishing Process

Shuo-Jen Lee[1], Yi-Ho Chen[1,], Jung-Chou Hung[2]*

[1]Department of Mechanical Engineering, Yuan Ze University,
[2]Mteal Industries Research & Development Centre
[*]E-mail: yihoyzu@gmail.com

As a popular application of electrochemical anodic dissolution, electropolishing is extensively adopted in the surface finishing industries of metals. Anodic dissolution is a complex reaction with many process parameters and chemical properties involved. A simple explanation of the mechanism of morphology formation during the EP reaction is still lacking. This study examines the morphology formation of stainless steel 304 at the same location on the specimen as the process evolves. Based on these observations, the basic mechanisms of morphology formation in EP process are proposed. The bubble shielding effect (BSE) and the broken bubble tunnelling effect (BBTE) explain the raised and dented morphologies, respectively. The broken bubble tunnelling effect (BBTE) explains the formation mechanism of pitting holes and the bubble shielding effect (BSE) explains the limitation of surface roughness of electropolishing process. Simulation results are consistent with the observed morphology formation phenomena.

1. INTRODUCTION

Electropolishing (EP) is an anodic method commonly adopted in industries to obtain a fine stress-free surface [1-2]. The driving mechanism of morphology formation during EP is important for anodic research and practical industrial applications [3-5]. Jacquet [6] pioneered EP research with a patent filed in 1930. Tegart [7] developed the reaction model and demonstrated some experimental results. In the 1950's, Hoar [8-11] and Edwards [12] investigated different electrolytes on various metals. According to the theory of Jacquet, applying a potential to a cell results in the formation of anodic film, viscous layer, over the surface of the anode. The film has a greater electrical resistance and viscosity than the bulk of the electrolyte solution, allowing it to manipulate the polishing

mechanism [13]. As shown in Figure 1(a), the resistance at the peaks of the rough surface is lower due to the thinner film. Since the current will travel along the path of least resistance, therefore, the peak at (A-B) will be dissolved faster than the valley at (C-D). It continues until the peaks are reduced to the level of the valleys.
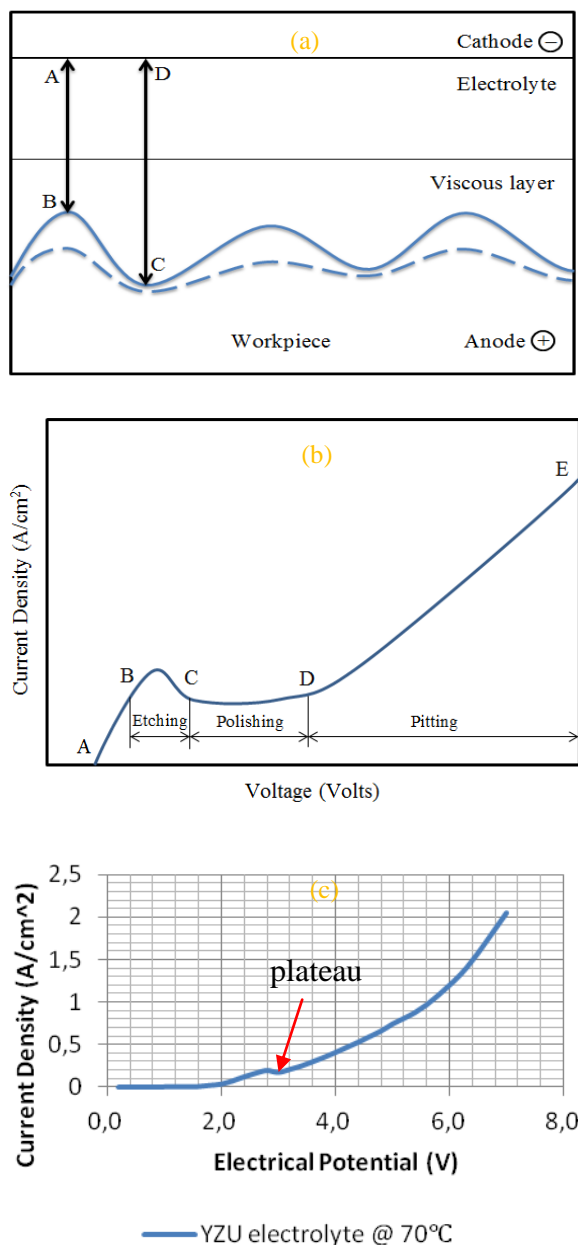
Figure 1. (a) Mechanism of electrolytic polishing proposed by Pierre Jacquet, (b) Fundamental current density-voltage curve for electropolishing [14], (c) I-V curve of SS304 (BA) EP in a mixture of phosphoric acid and sulfuric acid at 70℃

The expression from Jacquet is the first reaction model on surface morphology variation during electropolishing. Hahn and Marder [14] used the I-V curve to explain fundamental electrochemical characteristics. Regions on the I-V curve (Figure 1(b)) can be distinguished as: etching with an

unstable dissolution (B-C); stable plateau with polishing (C-D); and dissolution with pitting (D-E). In practical applications, although the EP process takes place in the plateau region, the pitting holes are still observed on the specimen after EP [15]. In this study, the pitting holes are not the corrosion pits due to the inclusion such as MnS in stainless steel but the results of an uneven anodic dissolution. To resolve this problem, the mechanism of morphology formation of EP should be investigated. Previous literatures have developed several mechanisms and/or models to explain the reaction of anodic dissolution: salt film (dissolution products) mechanism [16-17], acceptor mechanism [18], and preferential adsorption of shielding molecules mechanism [4-5]. In these models, the effects do not consider the massive number of bubbles on the anode. The bubbles are generated spontaneously and randomly during EP reaction. The dynamics of the bubbles is difficult to be observed. The numerical analysis is a better method to understand the formation and the collapse of the bubbles [19]. Their influences on electrical field distribution during EP reaction could also be studied. By using the commercial finite element method software, COMSOL Multi-physics, this study simulates how bubbles affect the morphology formation by computing the current density distribution on the surface of specimen coupled with moving mesh field to obtain the final morphology. The schematic of study flow is shown in Figure 2.
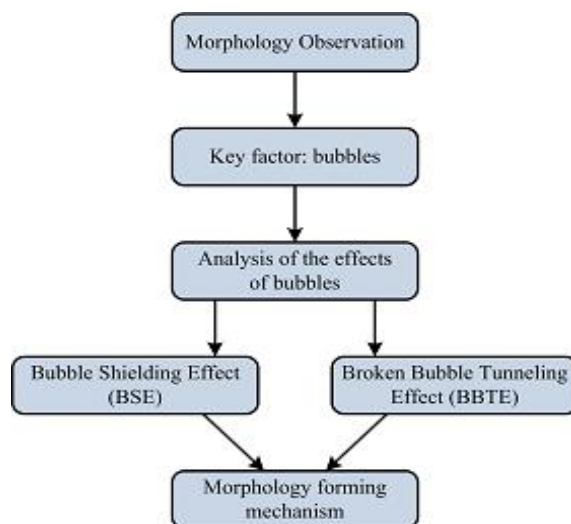
**Figure 2.** Schematic of study flow

2. OBSERVATIONS OF SURFACE MORPHOLOGY

This study investigates the mechanism of morphology formation, especially the formation of pitting holes during the EP process without stirring, by marking the SS-304(BA) specimens (50 mm x 70 mm) with deep scratches for an exact verification of location. The EP process is operated with the electrolyte (YZU electrolyte) of a mixture of phosphoric acid and sulphuric acid (4:1) [20-21]. In this study, the specimens, the anodes, are stainless steel SS304-BA (bright annealed) plates with R_a of 0.04 μm to 0.06 μm and R_p of 0.32 μm to 0.46 μm with a size of 50 mm x 80 mm. The specimens are degreased by Acetone with ultrasonic cleaning and then water rinses before EP. The cathode is a

stainless steel 304 mesh with the size of 60 mm x 90 mm. The inter-electrode gap is 10 mm. The I-V curve of the electropolishing reaction is measured, as shown in Figure 1(c). The applied voltage is set at 7 volt to obtain a pitting surface. At the 1st EP, two specimens are electropolished for 160 seconds and photographs of the surface morphology are taken. After the first observation, the 2nd EP is done again. The two specimens are electropolished again for additional 10 and 20 seconds, respectively. The 3rd EP takes additional 10 and 20 seconds again on the same specimen of the 2nd observation. Figure 3 shows the microscopy of the specimen surface of these three EPs. The pitting holes look like raised craters but the real shape of the pitting holes is concaved. Figure 4 shows the sectional profile measured by a confocal laser scanning microscopy. It reveals the formation of new pitting holes during the 2nd and 3rd stages, respectively. From these experiments, the following observations are made:

1. The pitting holes can be formed in a few seconds;
2. The pitting holes are formed randomly;
3. The shape of existing pitting holes is not changed by the following EP process;
4. The uneven dissolution is the driving mechanism of forming the concaved pitting holes.

From the above observations, the formation of pitting holes seems to have a close relationship with the bubbles generated near the specimen surface when escaping towards the bulk of electrolyte. Notably, the massive bubbles on the anode are oxygen. According to Faraday's Law of electrolysis, the mass of a substance altered on an electrode during electrolysis is directly proportional to the electricity transferred at the electrode.
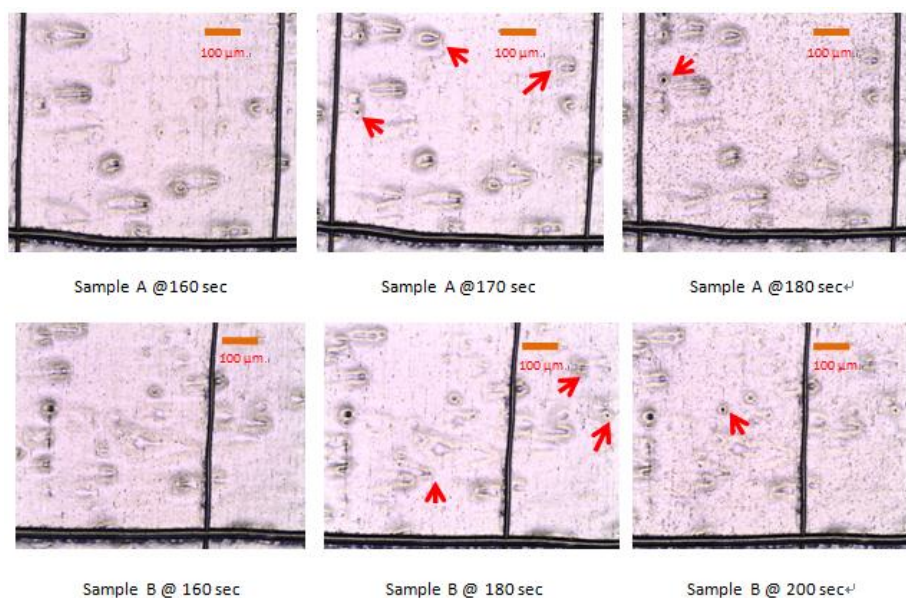
Figure 3. Pictures of surface morphology at different EP times (5x10) (The arrows indicate the new pitting holes.)

The current density distribution on a specimen determines the generation of the oxygen bubbles. It explains why more pitting holes on the edge of the specimen are generated where the current density distribution is higher than the rest of the area due to the edge effect. At the edges of a

conductor, the electrical field and the current density are normally high. To date, only the effects caused by bubbles during electrolysis could be observed. It still lacks an explicit physical model to explain the morphology formation on the anode in EP process. The commercial software, COMSOL Multiphysics, is used in this study to develop a reaction model to understand the effects of bubbles during EP.
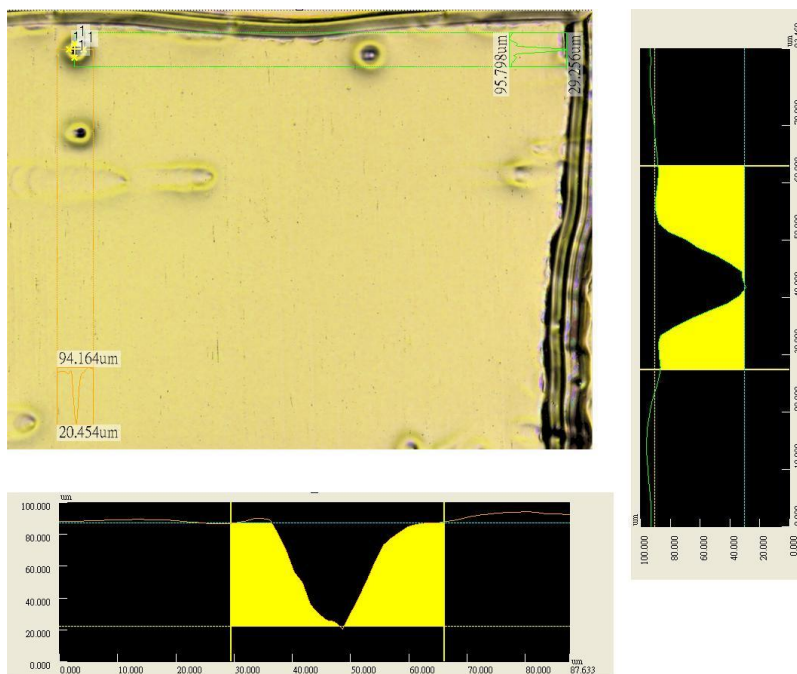
Figure 4. The cross-sectional profiles of a pitting hole measured by confocal laser scanning microscope

3. THEORETICAL MODEL AND NUMERICAL SIMULATION

During the electrolysis reaction, the effects of material property, electrolyte composition, current distribution and flow field are complex. To simplify the complexity of the electrolysis, the simulation is performed under the following conditions:

1.   According to the definition of electrical potential;

$$V = KQ / r \qquad (1)$$

Where K is the Coulomb's constant (K = 9 x10^9 N·m^2/C^2); Q is the charge amount; r is the curvature of the local surface morphology. The electrical charge distribution on a metal surface needs to be equal. Therefore, equation can be rewritten as:

$$Q = V \cdot r / K \qquad (2)$$

2.   The reaction obeys laws of electrochemical kinetics. The numerical simulation takes only the primary current distribution;

3.   We assume that the concentration of the electrolyte is uniform during EP in the simulation. According to Nernst's Theory, the polarization of electrochemical reaction mainly consists of two parts, concentration polarization and activation polarization. For an anodic dissolution, the concentration difference between the surface of metal anode and the electrolyte is huge, so only activation polarization counts;

4.   Conductivity of the electrolyte and viscosity of the viscous layer (anodic film) are uniform;

5.   Current efficiency of the electrolysis reaction is constant; and

6.   Material property of the specimen is uniform.

3.1 The Theoretical Model

The current density, i_n, is calculated by the charge distribution Q which is obtained from Equation (2).

$$i_n = Q / (A \cdot t) \qquad (3)$$

where t is the time ; A is the area.

The rate of moving mesh velocity, v, at which the anodic surface dissolved is determined by Faraday's law:

$$v = -k\, i_n \qquad (4)$$

$$k = M\theta / \rho z F \qquad (5)$$

where k is the constant of reaction efficiency; M is the molecular weight of the metal used as the anode; ρ is the density of the anode; z is the effective equivalent valence of the anode ; F is the Faraday's constant (F = 96,485 C/mol) ; and θ is the current efficiency of metallic dissolution, which is assumed to be constant at 70% in this study.

*3.2 Model Development*

Equation 4 is the governing equation of the moving mesh field of COMSOL. It can determine the mesh velocity, v, on the anodic surface. The mesh changes represent the morphology formation of the finite elements of the surface. Therefore, the mesh velocity, v, is proportional to the constant of the reaction efficiency, k, and the current density i_n. The final surface morphology of the specimen can be simulated according to the mesh velocity, v, and the reaction time.

3.3 Simulation of Bubble Shielding Effect (BSE)

A bubble with the size of 30 μm is simulated at different distances from the surface of the specimen to examine its effects and analyze the current density distribution on the surface. The bubble causes a shielding effect on the electrical field in the electrolyte. Restated, when the bubble is closer to the surface of the specimen, the current density distribution of the surface shielded by the bubble is around 2.1×10^1 A/cm^2 and the current density of the area without bubble shielding is around 2.5×10^1 A/cm^2. The values are read from Figure 5(a). This shows that the bubble shielding may lead to around 20% current density distribution deviation on the surface of a specimen. When the bubble is moved away from the surface, the extent to which bubble shielding affects the current density is diminished. Simulation results, as shown in Figure 5(a), indicate that the shielding effect diminishes and becomes negligible when the bubble is 4 times the size of its diameter away from the surface of the specimen and the lowest current density distribution is at the central bottom of the bubble. Lower current density distribution caused by the shielding of the bubble leads to a small protrusion or raised morphology on the surface, as shown in Figure 5(b), which contributes to the surface roughness of Ra. This finding may explain why the surface roughness of the EP process could only be as good as around 0.02 μm Ra and it also explains why longer polishing time, in the most cases, cannot provide better surface roughness [4-5].
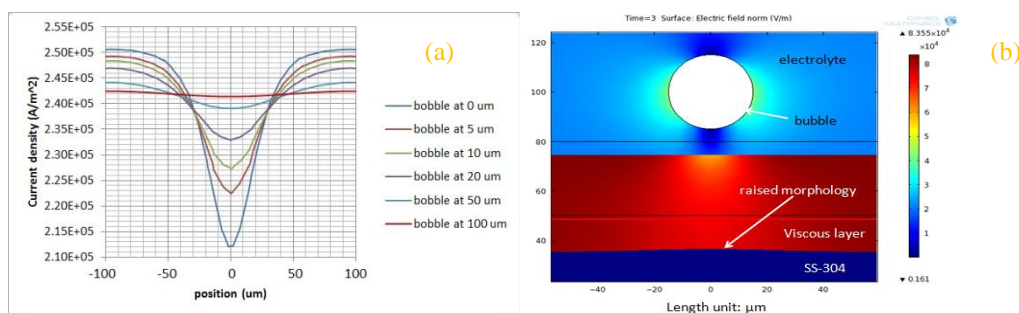
Figure 5. (a) The current density distribution on the surface of SS304 specimen caused by the shielding of the bubble with size of 30 μm at various distance from the surface, (b) The simulation model and the morphology formation by BSE

3.4 Simulation and Verification of the Broken Bubble Tunnelling effect (BBTE)

Close examination of the EP reaction, as shown in Figure 6, reveals that the bubbles can be generated in both the viscous layer and the electrolyte near the specimen. The bubbles shown in the viscous layer diffuse to the air and disappear within 8 seconds. This observation provides us a reference that BBTE should last for only a few seconds till the viscous layer returns to flat surface because of the surface tension. In EP reaction, when the bubble escapes from the viscous layer to the electrolyte, the viscosity difference between the viscous layer and the electrolyte could cause the bubble to break; in addition, the vacancy of the bubble is filled by the electrolyte, which has higher

fluidity than that of the viscous layer. During simulation, a broken bubble with a diameter of 30 μm is filled with the electrolyte, Figure 7(a). This figure reveals that the broken bubble creates a shorter path for the charges comparing to the locations without broken bubble in the viscous layer. Therefore, a tunnel seems to have twice the current density than that of the surrounding area. By the continuous current supply, a higher current density within the broken bubble tunnel increases the dissolution rate to the surface of the specimen. Therefore, a pitting hole is generated, as shown in Figures 7(b), 7(c) and 7(d). This phenomenon is referred to as the Broken Bubble Tunnelling Effect (BBTE). Next, the shape of a real pitting hole is compared with our simulation results, in which a SS304 specimen is electropolished by the same conditions of numerical simulation. Table 1 compares the simulation results with the experimental ones. The conductivity values showed in Table 1 are obtained by collecting the viscous layer and the electrolyte many times after EP and measured by conductivity meter, WTW-LF330. The thickness of the viscous layer is calculated by the weight difference of the specimen with and without the viscous layer. The simulated pitting hole diameter is 48 μm, with a depth of 53 μm as compared to the measured pitting hole diameter of 40 μm and depth of 66 μm. Although the exact size of the broken bubble that causes the pitting hole measured in this study cannot be determined, the simulation results are highly similar to the experimental ones.

Table 1. Boundary conditions and results of both simulation and experiments

Boundary settings & Results	Simulation	Experimental
Material of specimen	SS304	SS304
Applied voltage	7 V	7 V
Conductivity of the electrolyte	120 mS/cm	120 mS/cm
Conductivity of the viscous layer	38 mS/cm	38 mS/cm
Thickness of the viscous layer	30 μm	30 μm
Constant of reaction efficiency, k	2×10^{-11}	NA
Reaction time	10 sec	10 sec
Bubble size	30 μm	NA
Diameter of pitting hole	48 μm	40 μm
Depth of pitting hole	53 μm	66 μm

Figure 6. Bubbles in the viscous layer
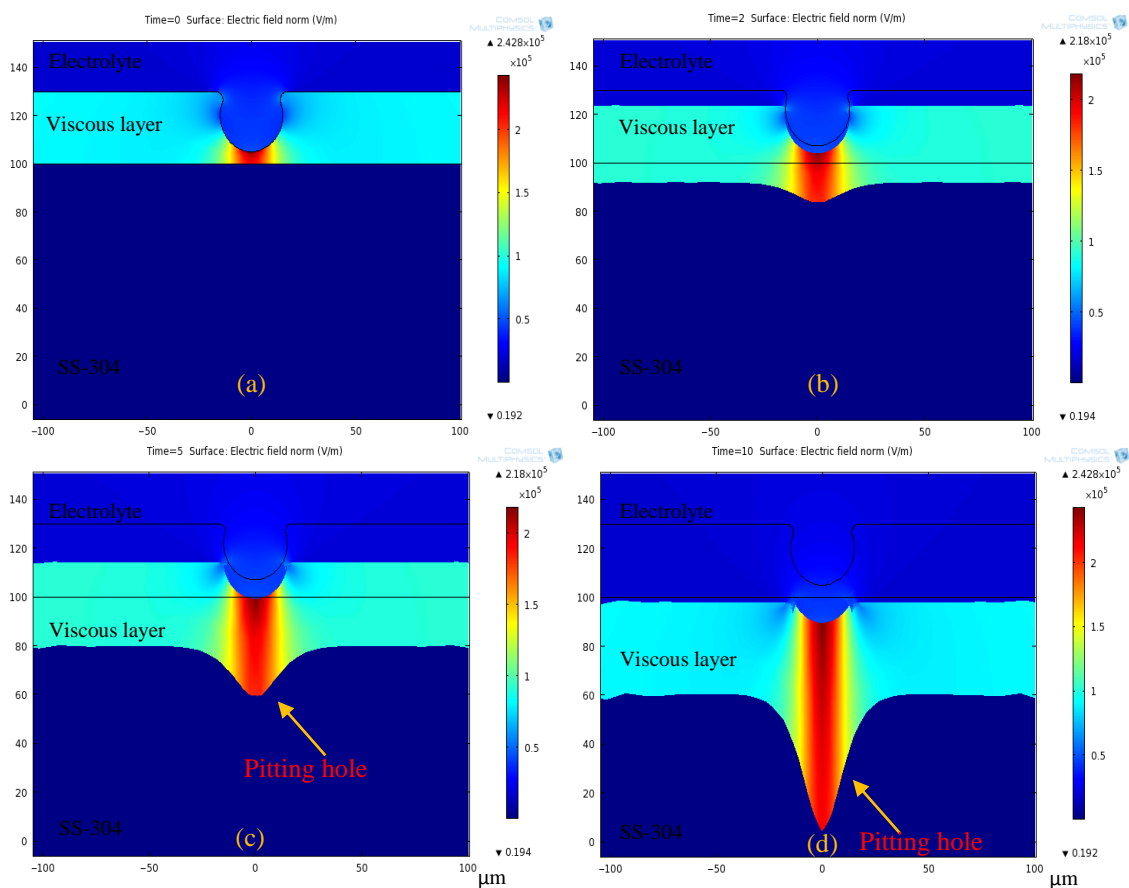
Figure 7. Simulation of Broken Bobble Tunnelling Effect: (a) time = 0, (b) time = 2 second, (c) time = 5 seconds, (d) time = 10 seconds

4. VERIFICATION EXPERIMENTS FOR BBTE

This study attempts to verify the BBTE theory and eliminate the formation of pitting holes during the EP reaction by performing some experimental runs with a pulsed power supply. According to the BBTE theory, the continuous current supply causes a deep etching to form the pitting hole if the dented viscous layer still exists. If the supply of the current before or during formation of the broken bubble can be stopped, the non-uniform etching mechanism is terminated because of termination of the electrochemical reaction. Therefore, the generation of the pitting holes could be reduced.

In order to verify the previous presumption, the pulsed current is applied for further experiments. Six experiments with various on-time settings of 10 seconds, 5 seconds and 2 seconds and off-time setting of 3 seconds and 1 second are tested under the same settings as the previous EP experiments. The total time of on-time setting is fixed at 100 seconds for the six experiments to ensure that the electrochemical reactions are performed at the same level. Table 2 lists the size distribution of the pitting holes, R_a and R_p under different current setting, while Figure 8 shows pictures of the surface morphology of the specimens. Experimental results indicate that some pitting holes still exist under the condition of 10 second and 5 second on-time. The size of pitting holes is distributed from 2 to 7 μm for the conditions of 2 second on-time. It becomes difficult to have a clear photo for these small pitting holes with the magnification of 20x10. Lowering the on-time setting decreases both values of the

diameter and the depth of the pitting holes. Above results are consistent with the BBTE theory. According to Faraday's laws of electrolysis, the mass of a substance altered at an electrode during electrolysis is directly proportional to the quantity of electricity transferred at the electrode. When the on-time is reduced, the size of the bubble and the generation of the bubbles during the reaction duty is also reduced. Therefore, the possibility of uneven anodic dissolution caused by BBTE is reduced and so will the formation of pitting holes.

According to the verification experiments, the EP reactions are under a voltage of 7 V, which is in the "pitting" range of Figure 1(a). By using a short pulse current with sufficient off-time, the pitting phenomenon can largely be eliminated. This finding reveals that the formation of pitting holes is due to a physical mechanism but not the defects of material itself or other chemical effects.
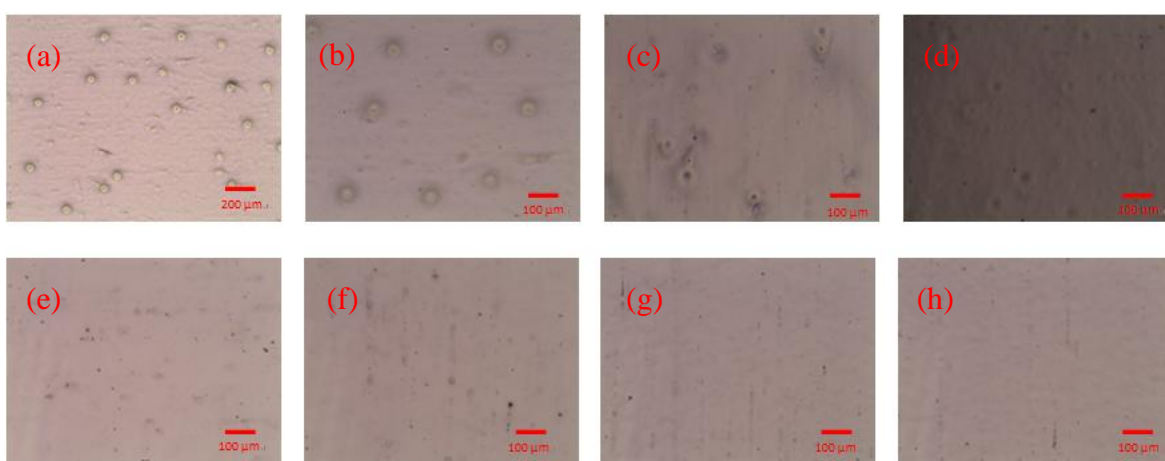
Figure 8. The microscopy picture of the specimens under different DC and pulsed current settings: (a) DC current EP 5 min. (10x10), (b) DC current EP 5 min. (20x10), (c) Pulse:10 sec. ON/ 1 sec. OFF (20x10), (d) Pulse:10 sec. ON/ 3 sec. OFF (20x10), (e) Pulse:5 sec. ON/ 1 sec. OFF (20x10), (f) Pulse:5 sec. ON/ 3 sec. OFF (20x10), (g) Pulse:2 sec. ON/ 1 sec. OFF (20x10), (h) Pulse:2 sec. ON/ 3 sec. OFF (20x10)

Table 2. The size distribution of pitting holes under different current setting measured by confocal laser scanning microscope

Current Setting	DC current	10 sec ON / 1 sec OFF	10 sec ON / 3 sec OFF	5 sec ON / 1 sec OFF	5 sec ON / 3 sec OFF	2 sec ON / 1 sec OFF	2 sec ON / 3 sec OFF
Diameter range (μm)	20~55	15~45	12~40	10~32	10~30	3~8	3~7
Depth range (μm)	30~70	10~45	8~30	5~15	4~14	2~7	2~6
R_a (μm)	0.58	0.47	0.45	0.36	0.34	0.12	0.10
R_p (μm)	3.96	3.88	3.85	2.26	2.02	0.62	0.42

5. DISSCUSSIONS

According to the theory developed by Jacquet, the difference in electrical resistance due to the variation of the anodic film (viscous layer) thickness is the main mechanism of planarization in electropolishing reaction. This model cannot explain the formation of the pitting holes and the effects of the massive amount of bubbles generated during the electropolishing reaction. For an electrochemical reaction, the reaction dynamics is from the applied electrical potential. This potential drives the electrical charges or electrons to move in the electrodes and the electrolyte. Once the electrons reached the surface of the anode, the distribution of the electrons should obey the equal potential principle on the surface of a conductor. Therefore, the sharp and raised morphology will attract more electrons and will have higher current density distribution. By Faraday's law of electrolysis, the higher current density at the sharp and raised morphology also has higher dissolution rate. Thence, the planarization is achieved. This is the planarization mechanism of electropolishing process we proposed in this study. It is different from the Jacquet's model and the Lin's model [4-5].

The effects caused by bubbles can be discussed in two parts, the complete bubble and the broken bubble. According to our observation, the bubbles could be generated in the electrolyte near the anode or in the viscous layer. If the bubbles are generated in the electrolyte, the bubbles will shield the electrical field and reduce the current density distribution on the surface of the anode. So, the dissolution rate of the anode where it is shielded by bubbles is reduced. If the bubbles are generated in the viscous layer, when the bubbles diffuse to the bulk of electrolyte, some of the bubbles will be broken because of the change in surface tension between the viscous layer and the electrolyte. Therefore, at the location where the bubble is broken, the viscous layer is thinner than elsewhere. Because the electrical resistance of the viscous layer is higher than the electrolyte, thence, the location with a broken bubble will form a low electrical resistance path and is named the Broken Bubble Tunnelling Effect in our study. This effect is the mechanism of forming pitting holes.

6. CONCLUSIONS

Based on the above simulation and experimental results, we conclude the following:

1.   Three mechanisms affect the current distribution on the surface of the specimen during the EP process. First, the micro-scale morphology deviation determines the charge distribution, which is governed by the edge effect. Second, the Bubble Shielding Effect (BSE) leads to a smaller dissolution rate and a raised morphology. Third, the Broken Bubble Tunnelling Effect (BBTE) causes a strong local dissolution, resulting in the formation of pitting holes;

2.   Formation of pitting holes is not related to material defects nor chemical effects;

3.   The Jacquet's model accurately describes the electropolishing reaction, yet fails to explain the phenomenon of morphology formation; and

4.   Electropolishing at the plateau region of the I-V curve is the better process window for smooth surface, because a lower reaction and less bubble formation also reduce BBTE.

Understanding the driving mechanism of surface morphology formation improves the ability to control surface morphology and to avoid the formation of pitting holes. Moreover, the desired surface morphology for different applications may be possible when using the electrochemical process.

References

1. T. Hryniewicz, R. Rokicki, K.Rokosz; *Surf. & Coatings Techno*. 64 (1994) 75-80.
2. A. Kutzlnigg, *Metallaberflache* 3 (1951) B67.
3. T. Tsure, *Materials Sci. and Eng*., A146 (1991) 1-14.
4. C.-C. Lin, C.-C. Hu, *Electrochimica Acta*, 53 (2008) 3356-3363.
5. C.-C. Lin, C.-C. Hu, T.-C. Lee, *Surf. & Coatings Techno*. 204 (2009) 448-454.
6. P.A. Jacquet, *French Patent No*. 707526 (1930).
7. W.J. Tegart, The Electrolytic and Chemical Polishing of Metals, Pergamon Press LTD, London (1959).
8. T.P. Hoar and J.A.S. Mowat, *Nature* 165 (1950) 64.
9. T.P. Hoar and T.W. *Farthing*, 169 (1952) 324.
10. T.P. Hoar, *Corros. Sci*. 7 (1967) 341.
11. T.P. Hoar and G.P. Rothwell, *Electrochimica Acta*, 9 (1964) 135.
12. J. Edward, *J. Electrochem. Soc*. 100 (1950) 198C-223C.
13. E. Weidman, Electrolytic Polishing, Metals Handbook, Ed. 9, Vol. 9, 48-56.
14. T.S. Hahn and A.R. Marder, *Metallography* 21 (1988) 365-375.
15. J.-J. Lai, The study of the mechanism of electropolishing process on SS316, Ph.D Thesis, Yuan Ze University, Taiwan, (2006).
16. V.V.Yuzhakov, H.C. Chang, A.E. Miller, *Phys. Rev*. B56 (1997) 608.
17. J.L. Hudson, T.T. Tsotsis, *Chemical Eng. Sci.,* 49 (1994) 1493-1572.
18. D. Landolt, *Electrochimica Acta* 32 (1987) 1.
19 M. Ohta, D. Daisuke, Y. Yoshida, M. Sussman, *Inter. J. of Multiphase Flow*, 39 (2011) 1059.
20 S. Magaino, M. Matlosz, D. Landolt, *J. Electrochem. Soc*. 140 (1993) 1365.
21 D.R. Gabe, *Corros. Sci*. 13 (1973) 175.